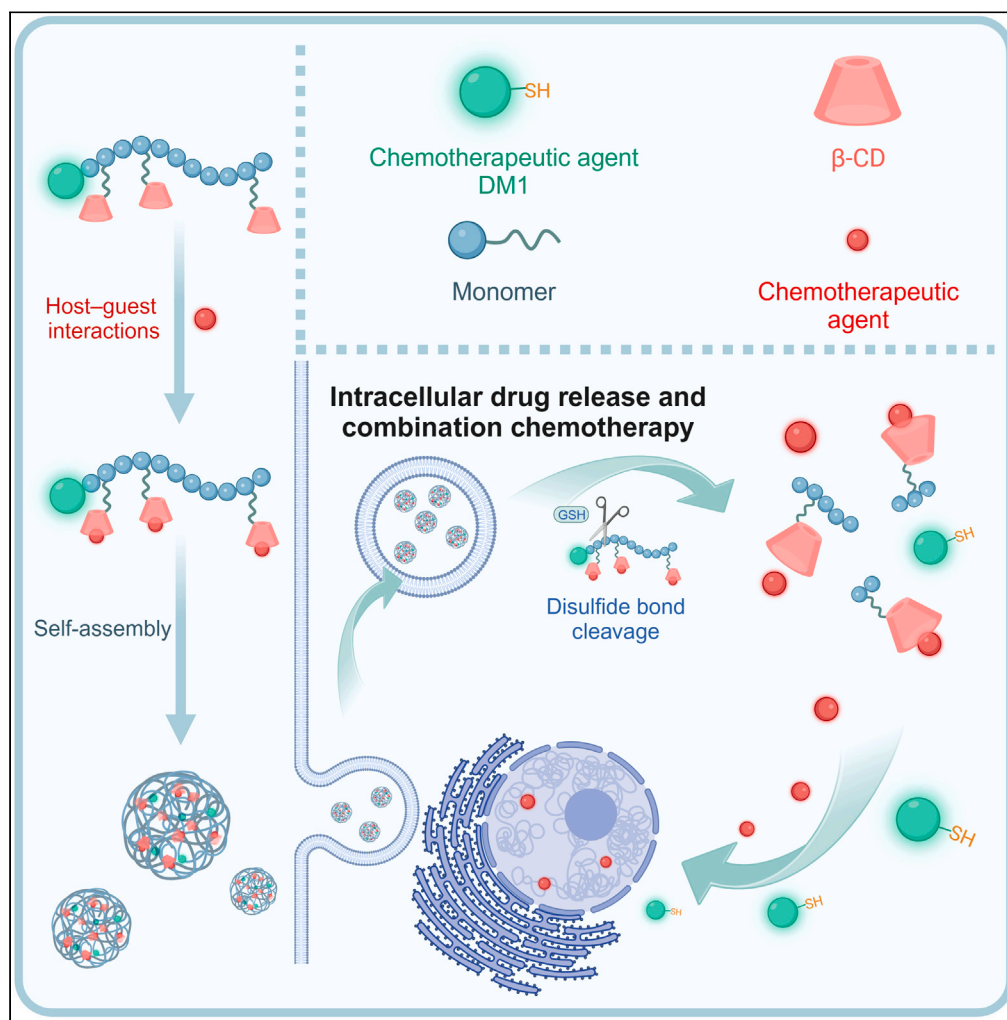**Article**

Drug-initiated poly(thiocitc acid) polymer incorporating host-guest interaction for cancer combination chemotherapy

Kai Yang, Bing Bai,
Feihe Huang,
Guocan Yu

fhuang@zju.edu.cn (F.H.)
guocanyu@mail.tsinghua.edu.
cn (G.Y.)

Highlights

Drug-initiated polymer for
precise control of
combination
chemotherapy

Host-guest complexation-
enhanced drug loading
capability

Completely degradable
and GSH-responsive
polymer

Article

Drug-initiated poly(thiocitc acid) polymer incorporating host-guest interaction for cancer combination chemotherapy

Kai Yang,[1,2,3] Bing Bai,[3] Feihe Huang,[1,2,*] and Guocan Yu[3,4,*]

SUMMARY

Combination chemotherapy has shown considerable promise for cancer therapy. However, the hydrophobicity of chemotherapeutic agents and the difficulties of precise drug co-administration severely hinder the development of combination chemotherapy. Herein, we develop a polymeric drug delivery system (D-PTA-CD) to provide robust loading capacity, glutathione-responsive drug release, and precise combination therapy. The vehicle is prepared based on poly(thioctic acid) (PTA) polymers using DM1, a chemotherapeutic agent, as the initiator to endow the vehicle with cancer-inhibiting activity. β-cyclodextrins are incorporated into the side chains to enhance drug loading capacity via host-guest interactions. Attributing to the sufficient disulfide bond on the backbone, D-PTA-CD exhibits accelerated drug release triggered by elevated glutathione levels. Doxorubicin (DOX) and camptothecin (CPT) are encapsulated by D-PTA-CD to afford the combination chemotherapy nanoparticles (NP), DOX-NP, and CPT-NP, respectively, which exhibit significant synergetic anti-cancer effects, highlighting the enormous potential of D-PTA-CD as a versatile drug delivery platform for cancer combination chemotherapy.

INTRODUCTION

Chemotherapy has emerged as one of the most effective strategies to prevent cancer cell proliferation.[1] Nonetheless, chemotherapy encounters two principal challenges. Firstly, the prolonged use of a single chemotherapy agent can induce drug resistance, resulting in diminished therapeutic effectiveness.[2–5] Combination therapy, harnessing diverse anti-cancer mechanisms to synergistically eradicate cancer cells, is an effective method to overcome drug resistance.[6,7] Secondly, most chemotherapy drugs suffer from poor solubility, low blood concentrations, short circulation times, and challenges in cellular uptake, impeding the attainment of therapeutic drug concentration at target sites and leading to side effects.[8] One strategy to tackle this quandary is the incorporation of drug delivery systems (DDSs), where drugs are encapsulated within DDSs to create nanoparticles, thereby augmenting drug solubility, and enhancing cellular uptake efficiency.[9–14] The utilization of DDSs for the delivery of multiple chemotherapy agents not only facilitates combination therapy but also amplifies drug utilization efficiency. However, precise control over drug ratios for combination therapy within DDSs remains a formidable challenge.[15,16] Distinct drugs possess unique chemical and physical properties, yielding intricate co-assembly scenarios that may render the actual drug ratios loaded within DDSs inadequate for achieving optimal therapeutic effects. Consequently, the development of a DDS with inherent therapeutic properties for combination chemotherapy represents an exceedingly promising strategy within the field of chemotherapy and DDSs.

Polymeric DDSs stand out from various DDSs due to their notable advantages in terms of controlled release, safety, and functionalization, making them promising candidates in cancer therapy research. By employing judicious structural design, polymeric DDSs can achieve precise control over drug release dynamics. For instance, materials containing disulfide bonds exhibit glutathione-responsive functionality, whereby the elevated glutathione (GSH) levels within tumor cells can cleave disulfide bonds, prompting the disassembly of nanoparticles and subsequent drug release.[17–19] Typically, the predominant driving force supporting polymeric materials to carry hydrophobic drugs is the hydrophobic interactions. Nonetheless, relying exclusively on hydrophobic interactions may not prove sufficient for fabricating stable nanodrugs that safeguard drug molecules against leakage.[20] Different from the weak hydrophobic interactions, host-guest recognitions, show higher strength between macrocyclic hosts and compatible guest molecules, providing a strong alternative for loading drugs.[21–23] In addition, the dynamic nature of host-guest recognition empowers DDS to realize controllable drug release in response to various stimuli. This interaction holds the potential to bolster the stability and drug-loading capacity of DDS. Cyclodextrins (CDs) represent a category of biocompatible macrocyclic hosts featuring cavities ranging in size from 4.7 Å to 10 Å and serve as reliable hosts for a diverse array of chemotherapeutic

[1]Stoddart Institute of Molecular Science, Department of Chemistry, Zhejiang University, Hangzhou 310027, P.R. China
[2]ZJU-Hangzhou Global Scientific and Technological Innovation Center, Zhejiang University, Hangzhou 311215, P.R. China
[3]Key Laboratory of Bioorganic Phosphorus Chemistry & Chemical Biology, Department of Chemistry, Tsinghua University, Beijing 100084, P.R. China
[4]Lead contact
*Correspondence: fhuang@zju.edu.cn (F.H.), guocanyu@mail.tsinghua.edu.cn (G.Y.)
https://doi.org/10.1016/j.isci.2024.109070
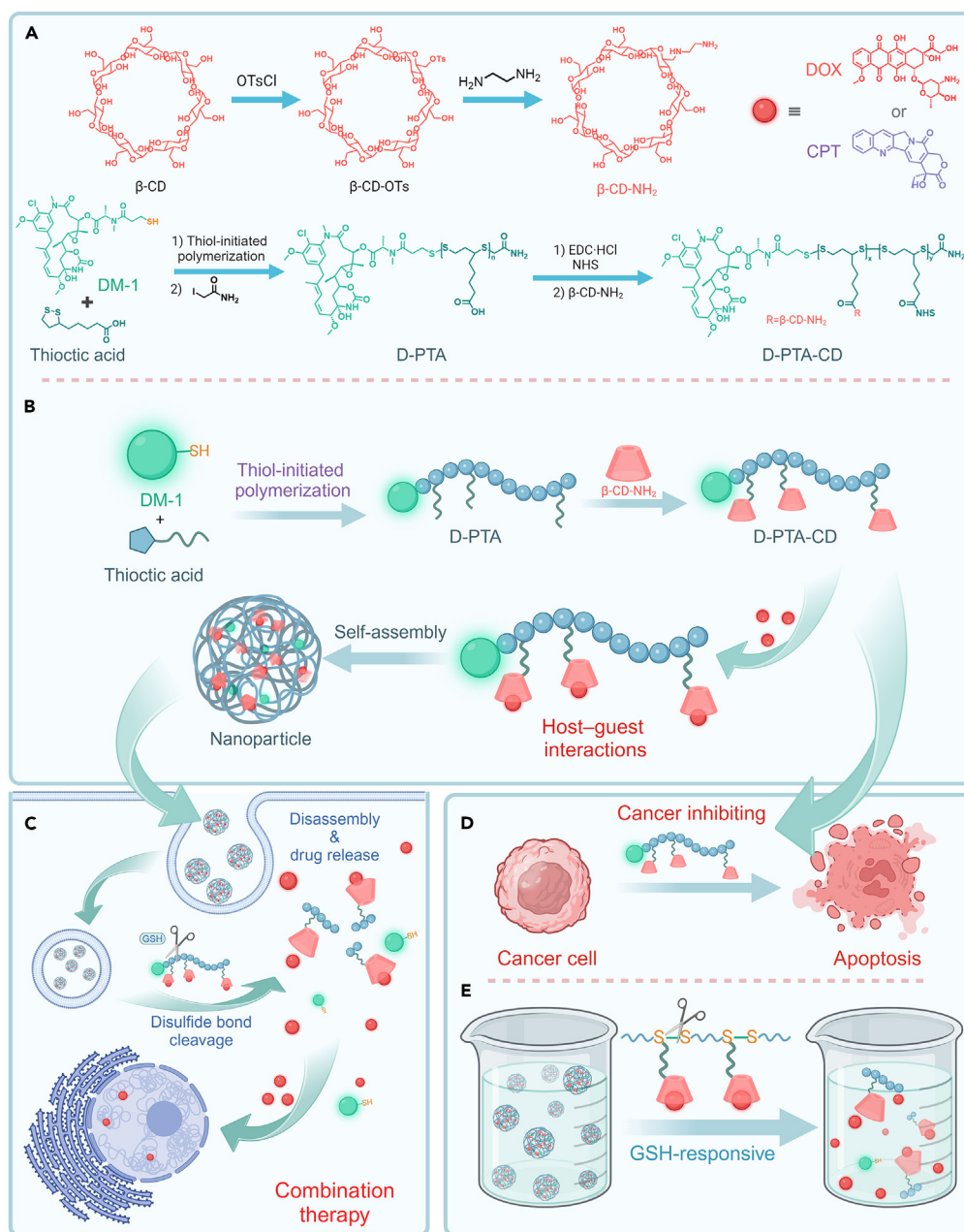
Scheme 1. Schematic illustration of the synthesis, self-assembly, GSH-responsive drug release, and therapeutic process

(A) Synthetic routes of the β-CD-NH$_2$ and D-PTA-CD.

(B) Schematic illustration of the thiol-initiated polymerization, host-guest interactions-mediated drug delivery.

(C) Intracellular therapy process including drug release and combination therapy.

(D) The cancer cell inhibition of D-PTA-CD.

(E) The GSH-responsiveness facilitates the disassembly of nanomedicines and drug release.

drugs.[24] Attributing to the robust host-guest interactions between CDs and drug molecules, the integration of CDs is poised to increase the drug loading content within DDS while further fortifying the stability of nanostructures.[25]

Herein, we develop a chemotherapeutic agent-initiated poly(thioctic acid) (PTA) DDS modified with β-CDs to provide precise and robust combination anticancer therapy (Scheme 1). The backbone is obtained through a ring-opening polymerization reaction initiated by the thiol on the chemotherapeutic agent, DM1, giving the DM1-initiated PTA (D-PTA). β-CDs are modified to the side chains of D-PTA to provide strong host-guest interactions to load additional chemotherapeutic agents. The loading capacity and stability of CD-modified D-PTA
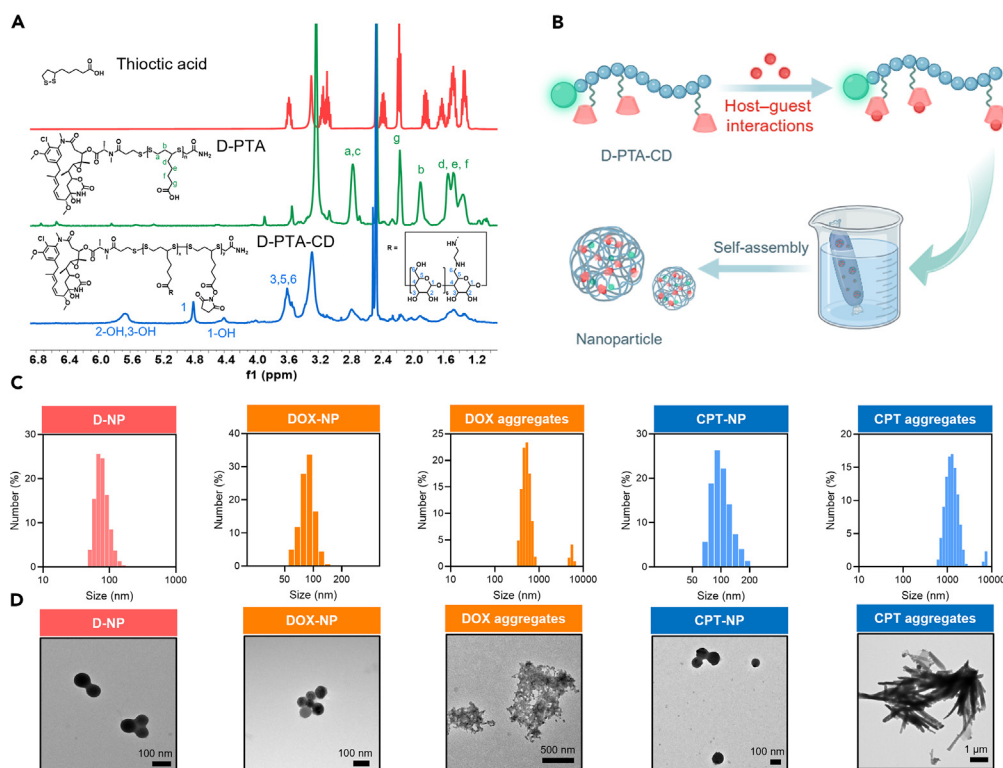
Figure 1. Characterizations of compounds and nanostructures

(A) ^{1}H NMR spectra of the thioctic acid, D-PTA, and D-PTA-CD.

(B) The drug delivery via host-guest interactions and the preparation of nanoparticles.

(C) DLS results of D-NP, DOX-NP, DOX aggregates, CPT-NP, and CPT aggregates.

(D) TEM images of D-NP, DOX-NP, DOX aggregates, CPT-NP, and CPT aggregates.

(D-PTA-CD) are promoted via the incorporation of host-guest interactions. Attributing to the microtubulin-inhibiting activity of DM1, the vehicle is tumor-inhibiting, presenting an anticancer platform for the combination therapy. Doxorubicin (DOX) and camptothecin (CPT) are loaded by D-PTA-CD, respectively, to fabricate the combinational therapeutic nanoparticles (NP), DOX-NP and CPT-NP, through a dialysis method. Both DOX-NP and CPT-NP exhibit excellent anti-cancer efficacy due to the remarkable synergetic effect of D-PTA-CD and the responsive drug release within the cancer cells. Taken together, this D-PTA-CD provides a new avenue of DDS for the fabrication of nanomedicines toward precise combination therapy.

RESULTS AND DISCUSSION

Synthesis and NP characterizations

D-PTA-CD was obtained through the reaction between D-PTA and β-CD-NH$_2$. Briefly, β-CD was activated by tosyl chloride to give the β-CD-OTs (Figures S1–S3), which then reacted with ethylenediamine to synthesize β-CD-NH$_2$ for the post-functionalization of D-PTA (Figures S4–S6). D-PTA was synthesized through a ring-opening polymerization of thioctic acid initiated by DM1 in methanol after heating at 60°C for 8 h. After the purification by diethyl ether, the material was fully characterized by ^{1}H NMR, ^{13}C NMR, and Fourier transform infrared (FTIR) spectroscopy (Figures S7–S9). According to the integration of the characteristic proton signals in the ^{1}H NMR spectrum, the degree of polymerization of D-PTA was calculated to be 20 and therefore the molecular weight of D-PTA was 4.9 kDa (Figure S7). After the polymerization, D-PTA was then activated by N-hydroxysuccinimide, followed by the reaction with β-CD-NH$_2$ to afford the D-PTA-CD (Figure 1A). The grafting number of CD was calculated to be 3 according to the ^{1}H NMR spectrum (Figure S10).

The critical aggregation concentration (CAC) of the amphiphilic D-PTA was determined to be 107.8 μg/mL by using pyrene as a probe (Figure S11). After the decoration of β-CD-NH$_2$, the CAC of D-PTA-CD was determined to be 101.2 μg/mL, suggesting no significant change of amphiphilicity occurred after the modification of β-CD (Figure S12). Nanoparticles of D-PTA-CD (D-NP), DOX-loaded D-PTA-CD (DOX-NP), and CPT-loaded D-PTA-CD (CPT-NP) were obtained via a dialysis method (Figure 1B). Transmission electron microscope (TEM) and dynamic light scattering (DLS) study were used to reveal the self-assembly of three nanoformulations. As depicted in the TEM image (Figure 1D), D-NP are solid sphere nanoparticles with a size of around 80 nm. The average size of D-NP was determined to be 79.2 ± 20.4 nm via DLS test (Figure 1C), consistent with the TEM result. After loading DOX or CPT, the average sizes were enlarged to 87.5 ± 17.1 nm for DOX-NP

and 103.1 ± 25.2 nm for CPT-NP (Figure 1C). In sharp contrast, hydrophobic DOX and CPT formed large aggregates in the absence of amphiphilic D-PTA-CD (Figures 1C and 1D). DOX formed sheet-like aggregates larger than 500 nm and fiber-like CPT aggregates larger than 1 μm were observed in the TEM, suggesting the poor solubility of CPT and DOX in an aqueous solution (Figures 1C and 1D). These aggregation behaviors of DOX and CPT further emphasized the necessity to employ DDS to improve the solubility of hydrophobic chemotherapeutic agents. In addition, the colloidal stability of the fabricated CPT-NP and DOX-NP was evaluated by tracking the change in average size after incubation in PBS over 48 h (Figure S13). No apparent variation was observed for both NPs, meaning that these drug-loaded NPs were stable.

Drug loading capacity evaluation and NP endocytosis study

The drug encapsulation efficiency (EE) was accessed to study the impact of host-guest interactions mediated by the β-CD in the vehicle via the UV-Vis spectrum. D-PTA was used as a control to encapsulate the hydrophobic CPT and DOX, affording the EE of 25.7% for CPT and 45.2% for DOX according to the standard curves (Figures S14 and S15), which suggested that the hydrophobic interactions alone were not sufficient to fabricate high-content nanomedications. Notably, in addition to the hydrophobic interactions between drugs and the PTA backbone, D-PTA-CD provided host-guest interactions between hydrophobic drugs and macrocyclic β-CDs as another driving force to facilitate the encapsulation of DOX and CPT. The host-guest interactions between DOX and β-CD in an aqueous solution were verified via ^{1}H NMR spectroscopy. As shown in Figure 2A, signals related to DOX protons turned broad after mixing the host and guest with a molar ratio of 1:3, which indicated the host-guest interaction. CPT is a hydrophobic chemotherapeutic agent that hardly solutes in aqueous solution, leading to obstacles in clinical use. Indeed, no CPT-related signal was observed in the ^{1}H NMR spectrum in D_2O (Figure 2B). Surprisingly, signals related to the aromatic protons on CPT were monitored in the mixture of CPT and β-CD-NH$_2$, which indicated the host-guest interactions between CPT and β-CD-NH$_2$ and further highlighted the enhanced solubility of CPT assisted by β-CD-NH$_2$ (Figure 2B). In addition, the host-guest interactions between CPT and β-CD-NH$_2$ were validated in the fluorescence spectra. The fluorescence intensity of CPT in aqueous solution was increased upon the addition β-CD-NH$_2$, which could be attributed to the disruption of π-π stacking after host-guest complexation (Figure 2C). Notably, compared to the poor solubility of free CPT (13.3 μg/mL), the incorporation of β-CD-NH$_2$ remarkably increased the solubility of CPT by 42.9 times, reaching 570 μg/mL (Figure 2D). Actually, the association constant for CPT and β-CD was determined to be $1.5 \times 10^4\,M^{-1}$ in our previous study.[26] These host-guest interactions between drug guests and the host offered an additional driving force for D-PTA-CD to load drug molecules, which would benefit the loading capacity and the stability of fabricated NPs. As a result, the EE of CPT-NP was calculated to be 48.8%, and the EE of DOX-NP was 70.0%, highlighting the enhancement in drug loading capacity boosted by the host-guest interactions.

After the encapsulation by D-PTA-CD, DOX-NP, and CPT-NP exhibited similar absorption spectra to those of the free molecules (Figures S16 and S17), giving rise to the confocal laser scanning microscopy (CLSM) study (Figure 2E). The cellular uptake efficiency study of DOX-NP and free DOX by B16 cancer cells using CLSM was performed. Compared to the free small molecular DOX which showed limited uptake by B16 cells, a higher intracellular accumulation of DOX-NP was observed in the treatment of DOX-NP. Strong fluorescence originating from DOX-NP was found located in the cytoplasm after 2 h incubation of DOX-NP while the free DOX-treated cells emitted weak fluorescence, indicating a higher uptake of DOX facilitated by DOX-NP. Similar results were obtained when elongated the incubation to 8 h. The promotion of cellular uptake of DOX can be attributed to the improved solubility of DOX via D-PTA-CD. A quantitative analysis of cellular DOX fluorescence intensity further revealed that the coincubation of DOX-NP significantly increased the internalization up to 2.92-fold of free DOX treatment within 2 h, which highlighted the impact of D-PTA-CD as DDS to increase the intracellular DOX concentration (Figure 2F).

Studies of controlled release and GSH-responsiveness

Nanomedicines should remain stable when in circulation to prevent the leakage of loaded drugs which will cause side effects. Once the nanoparticles were uptaken by cancer cells, encapsulated drugs should be released, allowing the chemotherapeutics to take effect. We next evaluated the controlled release of nanoformulations under various conditions. Considering the acidic microenvironment in cancer cells,[27] CPT-NP, and DOX-NP were sealed in dialysis bags and dialyzed in the PBS at pH 7.4, 6.0, and 5.0 for 48 h to evaluate the release performance. As shown in Figure 3A, in comparison with the 22.8% accumulative release of DOX-NP in PBS (pH = 7.4) solution after 20 h, treatment of PBS (pH = 5.0) slightly accelerated the release, and the accumulative release reached 35.9% within the same period. These release profiles revealed that acid conditions contributed to the release of loaded drugs. Additionally, the tumor microenvironment also features a high level of GSH, which can eliminate elevated reactive oxygen species to maintain the redox balance. GSH is capable of cleaving the disulfide bonds in the backbone of D-PTA-CD, giving rise to the accelerated disassembly of drug-loaded NPs and the following drug release (Figure 3C). To further mimic the release behavior of disulfide bond-sufficient NP under the stimulation of high-concentration cellular GSH, release tests in the GSH solution (1 mM and 10 mM) were conducted. Different from the slow release in PBS which reached 14.3% within 10 h, DOX-NP released 33.7%, and 51.7% of the loaded DOX in the presence of 1 mM and 10 mM GSH within the same period (Figure 3B). In addition, the accumulative drug release of CPT-NP reached 44.7% in 10 mM GSH solution within 10 h and increased to 54.7% at 32 h. Obviously, the incorporation of GSH significantly boosted the release of loaded drugs, attributing to the disruption of the disulfide bond which triggered the disassembly of NP. NMR spectra further verified the depolymerization of D-PTA via the treatment of GSH for 24 h. As shown in Figure 3D, broad proton peaks of D-PTA turned sharp ones with splitting details after the addition of GSH for 24 h, suggesting the depolymerization induced by GSH. The disassembly of CPT-NP and DOX-NP was further verified by DLS analysis and TEM. After GSH treatment for 24 h, the predominant particles of DOX-NP and CPT-NP turned larger ones with average size of more than 1 μm (Figures 3E and 3F). Large aggregates representing released DOX and CPT were found under TEM in samples of DOX-NP and CPT-NP after treatment of GSH (Figures 3E and 3F). Taken together, D-PTA-CD exhibited an intriguing dual-responsiveness of pH and GSH, facilitating the controllable drug release within cancer cells, which guaranteed the anticancer effect of loaded drugs.
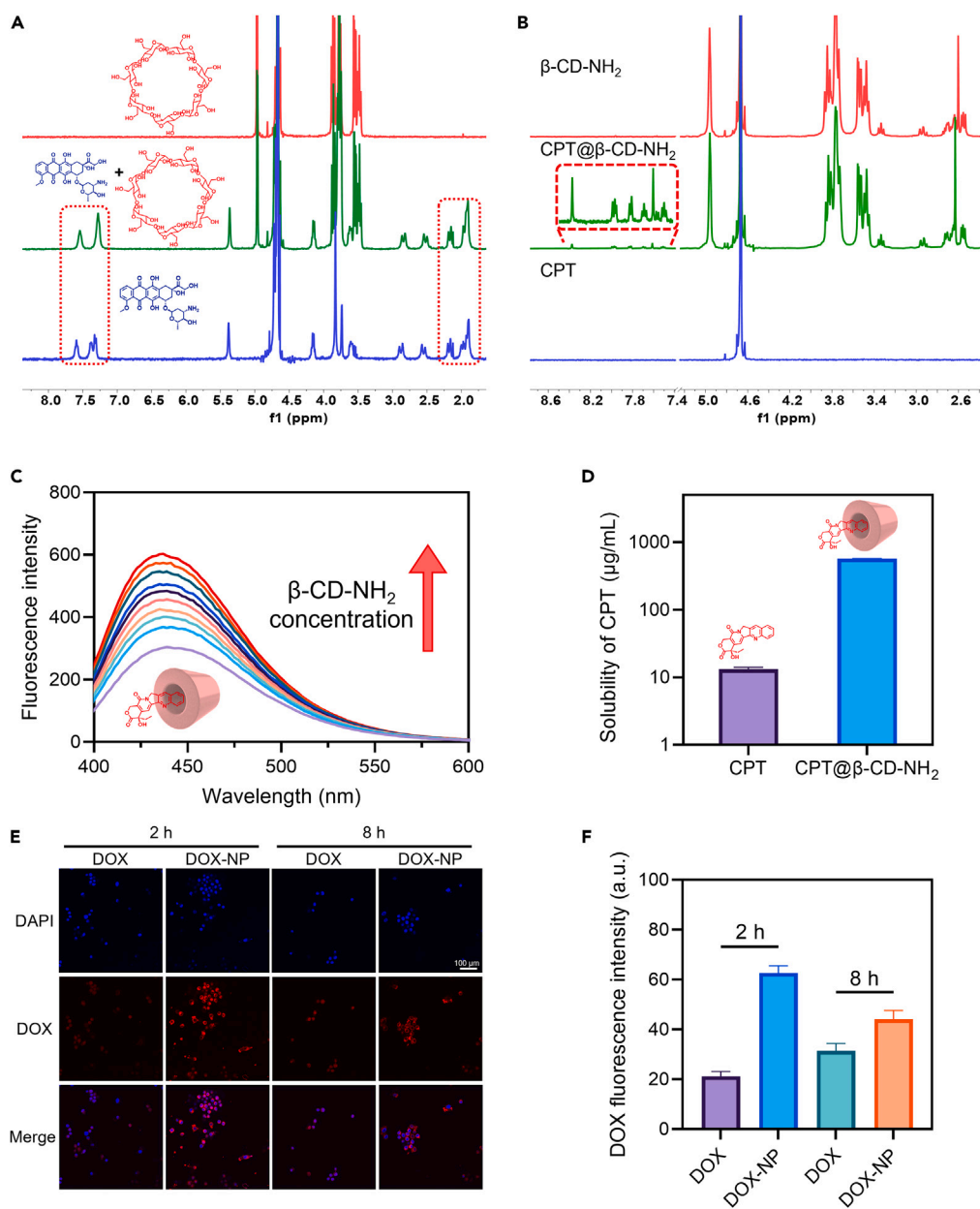
Figure 2. Host-guest interaction studies and endocytosis evaluation

(A) ^{1}H NMR spectra of the host-guest interactions between DOX and β-CD in D_2O.

(B) ^{1}H NMR spectra of the CPT, β-CD-NH$_2$, and their complex in D_2O. The inset indicates the aromatic protons on CPT in the CPT@β-CD-NH$_2$ complex.

(C) Fluorescence spectra of CPT in aqueous solution upon gradual addition of β-CD-NH$_2$.

(D) Solubility evaluation of CPT for free CPT and CPT@β-CD-NH$_2$. Data are presented as mean $\pm$ SD, n = 3 replicates.

(E) CLSM images of B16 after administration of DOX and DOX-NP for different time.

(F) Statistic DOX fluorescence intensity from (e). Data are represented as mean $\pm$ SD.

Combination chemotherapy evaluation

Although chemotherapy is a common treatment for many different cancers, single-agent therapy typically results in drug resistance and transient remission. Therefore, the combination chemotherapy employing distinct mechanisms is expected to overcome drug resistance and provide more effective anticancer efficacy. However, precise co-administration of multiple therapeutics remains a challenge due to the inefficient co-delivery strategy based on current non-therapeutic DDS. The drug loading efficiency varies depending on the chemical and physical properties of different chemotherapeutic agents. Moreover, the encapsulating scenario can be more complicated when intermolecular interactions
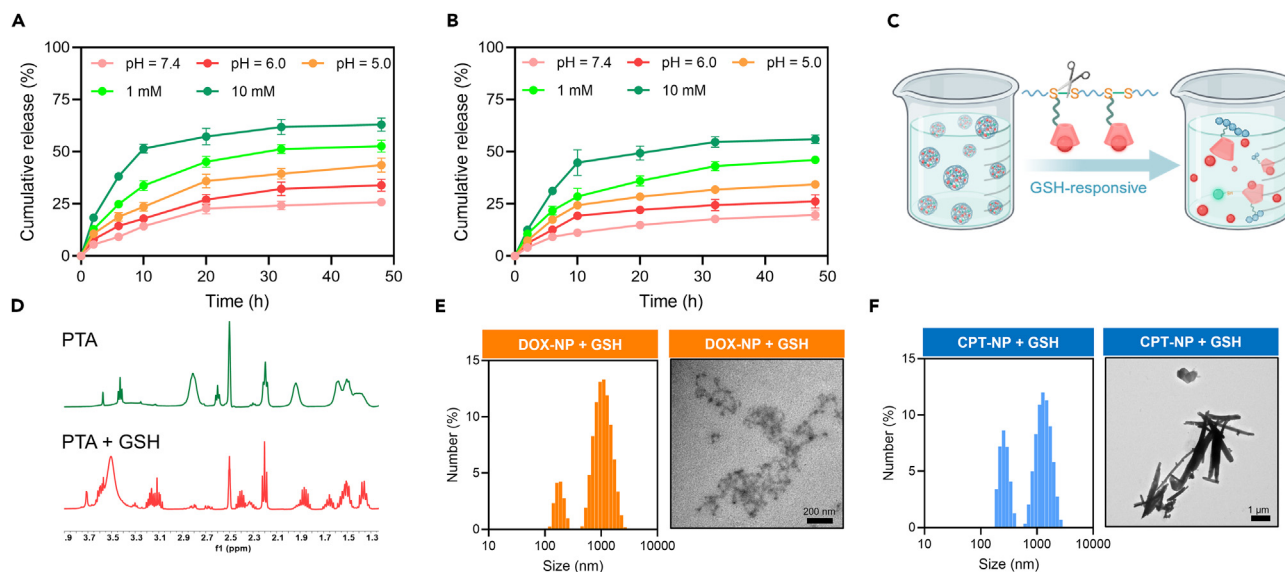
Figure 3. Release profiles of DOX-NP and CPT-NP and GSH-responsiveness studies

(A and B) Cumulative release profiles of DOX-NP (A) and CPT-NP (B) in various conditions. Data are presented as mean $\pm$ SD, n = 3 replicates.

(C) The disassembly mechanism of nanomedicines and drug release via GSH-responsiveness.

(D) ^{1}H NMR spectra of PTA before and after the treatment of GSH for 24 h.

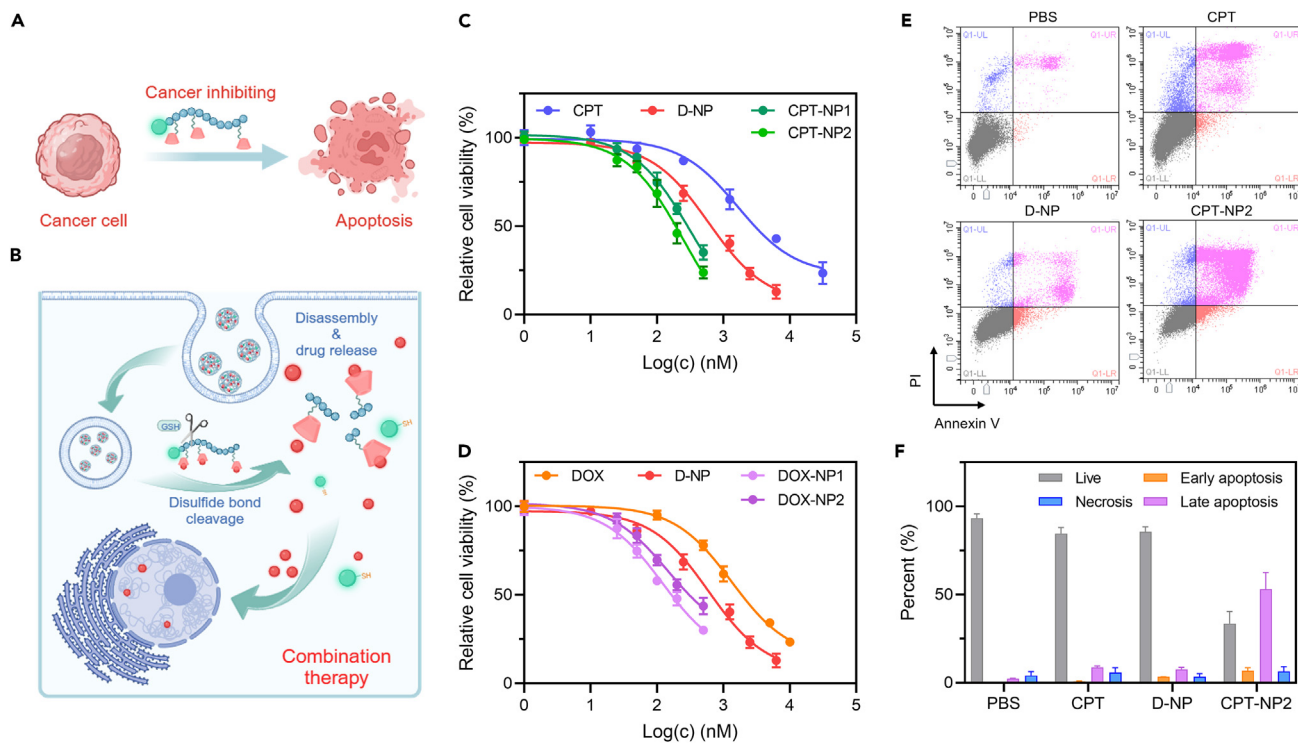(E) DLS results and TEM images of DOX-NP after treatment of GSH for 24 h.

(F) DLS results and TEM images of CPT-NP after treatment of GSH for 24 h.

occur between the combination agents, such as π-π stacking and electrostatic interactions, making it harder to manipulate the molar ratio of drugs for combination chemotherapy. Excitingly, D-PTA-CD, a therapeutic DDS for anticancer therapy, provides a facile and precise strategy to achieve combination therapy. By simply adjusting the loading content of loaded drugs, precise control of the combination formulation can be obtained to fuel the inhibition of cancer cells.

The anti-cancer efficacies of D-PTA-CD, DOX, and CPT were evaluated using a 3-(4′,5′-dimethylthiazol-2′-yl)-2,5-diphenyl tetrazolium bromide (MTT) assay. DM1 is an inhibitor of microtubule assembly, exhibiting half-maximal inhibitory concentrations (IC$_{50}$) of 645 nM (Figure S18). Due to the DM1 initiator, D-PTA-CD is a tumor-inhibiting polymeric DDS with IC$_{50}$ of 5.03 µg/mL, which was the equivalent of an effective DM1 concentration of 602 nM according to the molecular weight (Figure 4A). DOX and CPT are DNA topoisomerase inhibitors that stop DNA replication, showing IC$_{50}$ of 1.32 µM and 1.66 µM, respectively. Attributing to the distinct anti-cancer mechanism as well as GSH and pH-dual responsiveness, the combination of chemotherapeutic agents and D-PTA-CD exhibited excellent anti-cancer efficacy (Figure 4B). Two nanomedicines, CPT-NP1 and CPT-NP2 with various CPT loading content were prepared and administrated to B16 cells for 48 h. Since D-PTA-CD was a therapeutic DDS, the ratio of DM1 and CPT could be easily controlled in combination chemotherapy by adjusting the drug loading content. As shown in Figure 4C, CPT-NP1 achieved an IC$_{50}$ of 147 nM (measured by DM1 in D-PTA-CD), much lower than that of D-NP alone, and the combination index (CI) was 0.434, suggesting an s remarkable synergistic anti-cancer effect for CPT and D-PTA-CD (Figure 4C). CPT-NP2 with higher CPT content achieved an IC$_{50}$ of 120 nM with CI of 0.426. Similarly, strong synergetic effects and controllable combination chemotherapy were observed in the administration of DOX-NP. The CI for DOX-NP1 and DOX-NP2 was calculated to be 0.682 and 0.757, respectively, presenting D-PTA-CD as a universal combination therapy platform for anti-cancer combination chemotherapy (Figure 4D). Moreover, the synergistic effect of CPT-NP was further confirmed by the apoptosis study using Annexin V-FITC/propidium iodide (PI) assay. As shown in Figure 4E, combination chemotherapy using CPT-NP2 which simultaneously contained the D-PTA-CD and CPT induced 62.9% of apoptosis and necrosis. In sharp contrast, D-NP single treatment of comparable concentration in CPT-NP2 induced 11.2% of the cells to undergo apoptosis and necrosis after administration. Likewise, the ratio of apoptosis and necrosis cells induced by CPT single treatment reached 11.5%. Statistic flow cytometry (FCM) results revealed that the combination chemotherapeutic nanomedicine CPT-NP2 exhibited superior cancer cell inhibition over single treatments (Figure 4F), highlighting the potent synergistic anti-cancer effect of D-PTA-CD and CPT, and presenting the potential of D-PTA-CD for combination chemotherapy.

Conclusion

In summary, we developed a chemotherapeutic agent-initiated poly(thioctic acid) DDS with cyclodextrins on side chains, named D-PTA-CD, for robust drug delivery and precise combination chemotherapy. D-PTA-CD exhibited outstanding loading capacity via host-guest interactions between β-CD and drug guests. DOX-NP and CPT-NP, two nanoformulations for combination chemotherapy were constructed. The incorporation of D-PTA-CD greatly facilitated the cellular uptake efficiency and achieved controllable release in GSH-sufficient intracellular

Figure 4. Combination chemotherapy studies

(A) The cancer cell inhibition of D-PTA-CD.

(B) Intracellular therapy process including drug release and combination therapy using D-PTA-CD-based nanomedicines.

(C) MTT assays of CPT, D-NP, CPT-NP1, and CPT-NP2. Data are presented as mean $\pm$ SD, n = 5 replicates.

(D) MTT assays of DOX, D-NP, DOX-NP1, and DOX-NP2. Data are presented as mean $\pm$ SD, n = 5 replicates.

(E) Annexin V-FITC/PI staining of B16 after various treatments.

(F) Statistic results of Annexin V-FITC/PI staining of B16 after various treatments. Data are presented as mean $\pm$ SD, n = 3 replicates.

environment. Profiting from the cancer-inhibiting activity of D-PTA-CD, both DOX-NP and CPT-NP easily achieved precise combination chemotherapy and exhibited significant synergetic effect to inhibit cancer cell proliferation, presenting D-PTA-CD as a promising therapeutic DDS for precise combination chemotherapy.

Limitation of the study

In this study, the D-PTA-CD possesses excellent capability for precise combinational chemotherapy in B16 cell line when incorporated with CPT or DOX, however, more cancer cell lines should be included to comprehensively illustrate the feasibility of this strategy.

STAR★METHODS

Detailed methods are provided in the online version of this paper and include the following:

- ● KEY RESOURCES TABLE
- ● RESOURCE AVAILABILITY
  - ○ Lead contact
  - ○ Materials availability
  - ○ Data and code availability
- ● EXPERIMENTAL MODEL AND STUDY PARTICIPANT DETAILS
  - ○ Cell culture
- ● METHOD DETAILS
  - ○ Instruments and characterizations
  - ○ Synthesis of β-CD-NH$_2$
  - ○ Synthesis of D-PTA
  - ○ Synthesis of D-PTA-CD

- ○ Preparation of nanoparticles
- ○ Determination of encapsulation efficiency (EE)
- ○ DLS and TEM characterization
- ○ *In vitro* cell accumulation of the DOX-NP and DOX determined by confocal laser scanning microscopy (CLSM)
- ○ Evaluation of cytotoxicity
- ○ Determination of the combination index (CI)
- ○ Determination of the percentage of apoptotic cells at different stages by Annexin-V FITC/PI assay
- ● QUANTIFICATION AND STATISTICAL ANALYSIS

AUTHOR CONTRIBUTIONS

K.Y. performed the synthetic experiments carried out material characterization. B.B. carried out the biological experiments. K.Y., B.B., F.H., and G.Y. conceived the study and wrote the manuscript.

DECLARATION OF INTERESTS

The authors declare no competing interests.

REFERENCES

1. Konstantinopoulos, P.A., and Matulonis, U.A. (2023). Clinical and translational advances in ovarian cancer therapy. Nat. Cancer 4, 1239–1257. https://doi.org/10.1038/s43018-023-00617-9.

2. Fan, W., Yung, B., Huang, P., and Chen, X. (2017). Nanotechnology for Multimodal Synergistic Cancer Therapy. Chem. Rev. 117, 13566–13638. https://doi.org/10.1021/acs.chemrev.7b00258.

3. Pomeroy, A.E., Schmidt, E.V., Sorger, P.K., and Palmer, A.C. (2022). Drug independence and the curability of cancer by combination chemotherapy. Trends Cancer 8, 915–929. https://doi.org/10.1016/j.trecan.2022.06.009.

4. Zahreddine, H., and Borden, K.L.B. (2013). Mechanisms and insights into drug resistance in cancer. Front. Pharmacol. 4, 28. https://doi.org/10.3389/fphar.2013.00028.

5. Ward, R.A., Fawell, S., Floc'h, N., Flemington, V., McKerrecher, D., and Smith, P.D. (2021). Challenges and Opportunities in Cancer Drug Resistance. Chem. Rev. 121, 3297–3351. https://doi.org/10.1021/acs.chemrev.0c00383.

6. Palmer, A.C., and Sorger, P.K. (2017). Combination Cancer Therapy Can Confer Benefit via Patient-to-Patient Variability without Drug Additivity or Synergy. Cell 171, 1678–1691.e13. https://doi.org/10.1016/j.cell.2017.11.009.

7. Bookman, M.A., Brady, M.F., McGuire, W.P., Harper, P.G., Alberts, D.S., Friedlander, M., Colombo, N., Fowler, J.M., Argenta, P.A., De Geest, K., et al. (2009). Evaluation of New Platinum-Based Treatment Regimens in Advanced-Stage Ovarian Cancer: A Phase III Trial of the Gynecologic Cancer InterGroup. J. Clin. Oncol. 27, 1419–1425. https://doi.org/10.1200/jco.2008.19.1684.

8. Christidi, E., and Brunham, L.R. (2021). Regulated cell death pathways in doxorubicin-induced cardiotoxicity. Cell Death Dis. 12, 339. https://doi.org/10.1038/s41419-021-03614-x.

9. Elsabahy, M., Heo, G.S., Lim, S.-M., Sun, G., and Wooley, K.L. (2015). Polymeric Nanostructures for Imaging and Therapy. Chem. Rev. 115, 10967–11011. https://doi.org/10.1021/acs.chemrev.5b00135.

10. Shi, J., Kantoff, P.W., Wooster, R., and Farokhzad, O.C. (2017). Cancer nanomedicine: progress, challenges and opportunities. Nat. Rev. Cancer 17, 20–37. https://doi.org/10.1038/nrc.2016.108.

11. Chen, H., Zhang, W., Zhu, G., Xie, J., and Chen, X. (2017). Rethinking cancer nanotheranostics. Nat. Rev. Mater. 2, 17024. https://doi.org/10.1038/natrevmats.2017.24.

12. Wicki, A., Witzigmann, D., Balasubramanian, V., and Huwyler, J. (2015). Nanomedicine in cancer therapy: Challenges, opportunities, and clinical applications. J. Control. Release 200, 138–157. https://doi.org/10.1016/j.jconrel.2014.12.030.

13. Tong, R., Tang, L., Ma, L., Tu, C., Baumgartner, R., and Cheng, J. (2014). Smart chemistry in polymeric nanomedicine. Chem. Soc. Rev. 43, 6982–7012. https://doi.org/10.1039/C4CS00133H.

14. Li, Z., Song, N., and Yang, Y.-W. (2019). Stimuli-Responsive Drug-Delivery Systems Based on Supramolecular Nanovalves. Matter 1, 345–368. https://doi.org/10.1016/j.matt.2019.05.019.

15. Duan, X., Xiao, J., Yin, Q., Zhang, Z., Yu, H., Mao, S., and Li, Y. (2013). Smart pH-Sensitive and Temporal-Controlled Polymeric Micelles for Effective Combination Therapy of Doxorubicin and Disulfiram. ACS Nano 7, 5858–5869. https://doi.org/10.1021/nn4010796.

16. Zheng, M., Yue, C., Ma, Y., Gong, P., Zhao, P., Zheng, C., Sheng, Z., Zhang, P., Wang, Z., and Cai, L. (2013). Single-Step Assembly of DOX/ICG Loaded Lipid–Polymer Nanoparticles for Highly Effective Chemo-photothermal Combination Therapy. ACS Nano 7, 2056–2067. https://doi.org/10.1021/nn400334y.

17. Yang, H., Shen, W., Liu, W., Chen, L., Zhang, P., Xiao, C., and Chen, X. (2018). PEGylated Poly(α-lipoic acid) Loaded with Doxorubicin as a pH and Reduction Dual Responsive

Nanomedicine for Breast Cancer Therapy. Biomacromolecules 19, 4492–4503. https://doi.org/10.1021/acs.biomac.8b01394.

18. Zhang, X., Han, L., Liu, M., Wang, K., Tao, L., Wan, Q., and Wei, Y. (2017). Recent progress and advances in redox-responsive polymers as controlled delivery nanoplatforms. Mater. Chem. Front. 1, 807–822. https://doi.org/10.1039/C6QM00135A.

19. Liu, Y., Wu, Y., Luo, Z., and Li, M. (2023). Designing supramolecular self-assembly nanomaterials as stimuli-responsive drug delivery platforms for cancer therapy. iScience 26, 106279. https://doi.org/10.1016/j.isci.2023.106279.

20. Ma, X., and Zhao, Y. (2015). Biomedical Applications of Supramolecular Systems Based on Host–Guest Interactions. Chem. Rev. 115, 7794–7839. https://doi.org/10.1021/cr500392w.

21. Zhou, J., Yu, G., and Huang, F. (2017). Supramolecular chemotherapy based on host-guest molecular recognition: a novel strategy in the battle against cancer with a bright future. Chem. Soc. Rev. 46, 7021–7053. https://doi.org/10.1039/c6cs00898d.

22. Zhou, J., Rao, L., Yu, G., Cook, T.R., Chen, X., and Huang, F. (2021). Supramolecular cancer nanotheranostics. Chem. Soc. Rev. 50, 2839–2891. https://doi.org/10.1039/d0cs00011f.

23. Cheng, H.B., Zhang, Y.M., Liu, Y., and Yoon, J. (2019). Turn-On Supramolecular Host-Guest Nanosystems as Theranostics for Cancer. Chem 5, 553–574. https://doi.org/10.1016/j.chempr.2018.12.024.

24. Zhang, Y.M., Xu, X., Yu, Q., Yu, H.J., and Liu, Y. (2019). Drug Displacement Strategy for Treatment of Acute Liver Injury with Cyclodextrin-Liposome Nanoassembly. iScience 15, 223–233. https://doi.org/10.1016/j.isci.2019.04.029.

25. Zhang, Y.M., Liu, Y.H., and Liu, Y. (2020). Cyclodextrin-Based Multistimuli-Responsive Supramolecular Assemblies and Their Biological Functions. Adv. Mater. 32, e1806158. https://doi.org/10.1002/adma.201806158.

26. Yang, K., Qi, S., Yu, X., Bai, B., Zhang, X., Mao, Z., Huang, F., and Yu, G. (2022). A Hybrid Supramolecular Polymeric Nanomedicine for Cascade-Amplified Synergetic Cancer Therapy. Angew. Chem. Int. Ed. 61, e202203786. https://doi.org/10.1002/anie.202203786.

27. Peng, S., Xiao, F., Chen, M., and Gao, H. (2022). Tumor-Microenvironment-Responsive Nanomedicine for Enhanced Cancer Immunotherapy. Adv. Sci. 9, e2103836. https://doi.org/10.1002/advs.202103836.

28. Li, H., Peng, K., Yang, K., Ma, W., Qi, S., Yu, X., He, J., Lin, X., and Yu, G. (2022). Circular RNA cancer vaccines drive immunity in hard-to-treat malignancies. Theranostics 12, 6422–6436. https://doi.org/10.7150/thno.77350.

STAR★METHODS

KEY RESOURCES TABLE

REAGENT or RESOURCE	SOURCE	IDENTIFIER
Antibodies		
YF 488-Annexin V/PI	US EVERRIGHT	Cat#Y6002L
Chemicals, peptides, and recombinant proteins		
Thioctic acid	Meryer	Cat#M026347-500g
Camptothecin (CPT)	Bidepharm	Cat#BSL976
Doxorubicin hydrochloride (DOX·HCl)	Bidepharm	Cat#BGW591
Experimental models: Cell lines		
B16-F10	Laboratory of Prof. Xin Lin (Tsinghua University)[28]	Theranostics 2022; 12(14):6422–6436.
Software and algorithms		
GraphPadPrism 9.5	GraphPad	https://www.graphpad.com/
ImageJ	ImageJ	https://imagej.net/ij/

RESOURCE AVAILABILITY

Lead contact

Further information and requests for resources and reagents should be directed to and will be fulfilled by the lead contact, Guocan Yu (guocanyu@mail.tsinghua.edu.cn).

Materials availability

This study did not generate new unique reagents.

Data and code availability

- All data reported in this paper will be shared by the lead contact upon request.
- This paper does not report original code.
- Any additional information required to reanalyze the data reported in this paper is available from the lead contact upon reasonable request.

EXPERIMENTAL MODEL AND STUDY PARTICIPANT DETAILS

Cell culture

B16-F10 cell line was a kind gift from Prof. Xin Lin' Lab (Tsinghua University).[28] The cell line was commercially authenticated via short tandem repeat profiling, which was performed by the Xiamen Immocell Biotechnology Co., Ltd., and no mycoplasma contamination was found.

Cells were cultured in RPMI-1640 medium supplemented with 10% FBS and 1% antibiotic solution. Media were purchased from Gibco (Thermo Fisher Scientific). Cell cultures were maintained at 37°C with 5% CO_2. The cells were cultured in suitable plates for subsequent experiments.

METHOD DETAILS

Instruments and characterizations

^{1}H NMR spectra were recorded on a JNM-ECZ400S/L1. MTT cytotoxicity assay kits for cell viability detection were bought from Thermo Fisher Scientific. Transmission electron microscopy (TEM) investigations were carried out on an HT-7700 instrument. UV-vis absorption spectra were recorded by using an Agilent Cary 60 UV-vis spectrophotometer. Fluorescence spectra were recorded by using an Agilent Cary Eclipse. Confocal laser scanning microscopy (CLSM) images was recorded on an Olympus FV3000 microscope. The sizes of the nanoformulations were measured by a DLS analyzer (Zetasizer Nano ZS90 Malvern Instruments, Malvern) with a detection angle of 90° at 25°C using an incident He-Ne laser (λ = 633 nm).

Synthesis of β-CD-NH$_2$

β-CD (11.4 g, 10 mmol) and tosyl chloride (1.91 g, 10 mmol) were dissolved in 100 mL of anhydrous DMSO. Triethylamine (2.02 g, 20 mmol) in 10 mL DMSO was added dropwise into the solution. The solution was heated under stirring at room temperature for 24 h, after which the reaction was poured into 500 mL water. Precipitate was collected and washed by water twice and then washed by acetone, followed by evaporation under vacuum to give the β-CD-OTs (5.17 g, 40.0%) which was used without further purification. The ^{1}H NMR, ^{13}C NMR and mass spectra of β-CD-OTs are shown in Figures S1–S3.

β-CD-OTs (2.57 g, 2.00 mmol) and ethylenediamine (0.601 g, 10.0 mmol) were dissolved in DMSO and heated at 60°C under stirring. After heating for 24 h, the reaction was poured into acetone to move DMSO and ethylenediamine. The precipitate was washed by acetone for three times and then evaporated in vacuum to give the β-CD-NH$_2$ (1.95 g, 83.0%). The ^{1}H NMR, ^{13}C NMR and mass spectra of β-CD-NH$_2$ are shown in Figures S4–S6.

Synthesis of D-PTA

DM1 (74.8 mg, 100 μmol) and thioctic acid (1.24 g, 6 mmol) were dissolved in 2 mL MeOH. The reaction was heated at 60°C in N$_2$ atmosphere under stirring. After heating for 24 h, the reaction turned viscous liquid and was precipitated by diethyl ether for three times, followed by evaporation in vacuum. The ^{1}H NMR, ^{13}C NMR and FTIR spectra of D-PTA are shown in Figures S7–S9.

Synthesis of D-PTA-CD

D-PTA (200 mg), EDC (383.4 mg, 2.00 mmol), NHS (230 mg, 2.00 mmol), and DMAP (24.4 mg, 0.200 mmol) were dissolved in 5 mL anhydrous DMSO and stirred at room temperature. After stirring for 24 h, β-CD-NH$_2$ (1.5 g) was added to the reaction and kept stirring for 24 h. After the reaction, the solution was dialyzed (3500 Da MWCO) against deionized water. The polymer was then lyophilized to afford the D-PTA-CD. The ^{1}H NMR spectrum of D-PTA-CD is shown in Figure S10.

Preparation of nanoparticles

D-NP, CPT-NP and DOX-NP were prepared through a dialysis method. Briefly, D-PTA-CD (5.00 mg) was dissolved in 1 mL DMSO. Then, the solution was sealed in dialysis bag with an MWCO of 3.5 kDa and dialyzed against deionized water for 8 h to afford D-NP. For the preparation of DOX-NP, D-PTA-CD (5.00 mg), DOX·Cl and triethylamine were dissolved in 1 mL DMSO. Then, the solution was sealed in dialysis bag with an MWCO of 3.5 kDa and dialyzed against deionized water for 8 h to afford DOX-NP. For the preparation of CPT-NP, D-PTA-CD (5.00 mg) and CPT were dissolved in 1 mL DMSO. Then, the solution was sealed in dialysis bag with an MWCO of 3.5 kDa and dialyzed against deionized water for 8 h to afford CPT-NP. For the aggregates of CPT or DOX, CPT or DOX were dissolved in THF and dialyzed against deionized water for 8 h to obtain their aggregates.

Determination of encapsulation efficiency (EE)

The standard curves of CPT and DOX in DMSO were obtained using a UV-vis spectrophotometer (Figures S11 and S12). 100 μL of CPT-NP or DOX-NP was diluted by 900 μL DMSO to disrupt the structure of nanoparticle and release the loaded drugs. Then, the absorbance of CPT-NP or DOX-NP was measured and the concentration of DOX or CPT could be obtained according to the standard curves.

Encapsulation efficiency (%) = $m_{drug-ini} \div m_{drug-loaded} \times 100\%$ Where the $m_{drug-ini}$ is the mass of drug added to preparation the nanoparticles and $m_{drug-loaded}$ is the mass of encapsulated drug in the nanoparticles.

DLS and TEM characterization

The size distribution of dialyzed NPs was measured using a Zetasizer Nano ZS90 (Malvern Instruments). Samples were diluted 10 times by deionized water and 1 mL of the diluted NPs was transferred to a DLS cuvette for data acquisition.

The TEM characterization was carried out on an HT-7700 instrument. The obtained NPs was diluted 100 times by deionized water. 5 μL sample solution was applied to the electron microscopy grid and kept in vacuum at room temperature to evaporate water.

In vitro cell accumulation of the DOX-NP and DOX determined by confocal laser scanning microscopy (CLSM)

B16 cells were treated with the the DOX-NP and DOX (the concentration of DOX was kept at 1.00 μM) in the culture medium at 37°C for 2 h, and 8 h, respectively. The cells were washed three times with PBS and fixed with fresh 4.0% formaldehyde at room temperature for 15 min. After washing with PBS, the cells were stained with DAPI (1.00 μg/mL) for 15 min. The images were taken using an Olympus FV3000 microscope.

Evaluation of cytotoxicity

The cytotoxicity of the different formulations against B16 cells was determined by MTT assays in a 96-well cell culture plate. All solutions were sterilized by filtration with a 0.22 μm filter before tests. B16 cells were seeded at a density of 1.0 × 10^4 cells per well in a 96-well plate, and incubated for 24 h for attachment. Cells were then incubated with free CPT, DOX, DM1, D-NP, DOX-NP, or CPT-NP at different concentrations for 48 h. After washing the cells with PBS buffer, 20 μL of an MTT solution (5 mg/mL) and 180 μL of media were added to each well. After

4 h of incubation at 37°C, the MTT solution was removed, and the insoluble formazan crystals that formed were dissolved in 100 μL of dimethyl sulfoxide (DMSO). The absorbance of the formazan product was measured at 570 nm using a spectrophotometer. Untreated cells in media were used as a control. All experiments were carried out with five replicates.

Determination of the combination index (CI)

A series of combination chemotherapeutic nanomedicines with different ratios of D-PTA-CD and drugs were prepared by controlling the loading content. Different mass of drugs were added to the D-PTA-CD solution in DMSO and the solution was dialyzed to prepare corresponding NPs. The concentration of loaded drugs was determined by calculating the EE and all the D-PTA-CD was assumed to remain in the dialysis bag. The molar ratios of CPT and DM1 in CPT-NP1 and CPT-NP2 were determined to be 1.72:1 and 2.51:1. The molar ratio of DOX and DM1 in DOX-NP1 and DOX-NP2 were determined to be 1.67:1 and 0.772:1.

The CI value was calculated as follows: $CI = D_1/D_{f1} + D_2/D_{f2}$. Where D_{f1} is the dose of CPT or DOX required to produce x percent effect alone and D_1 is the dose of CPT or DOX required to produce the same x percent effect in combination with D-PTA-CD. Similarly, D_{f2} is the dose of D-NP required to produce x percent effect alone and D_2 is the dose of D-NP required to produce the same x percent effect in combination with CPT or DOX. Theoretically, CI is the ratio of the combination dose to the sum of the single-drug doses at an isoeffective level. Consequently, CI values of <1 indicate synergism, values of >1 show antagonism, and values of = 1 indicate additive effects.

Determination of the percentage of apoptotic cells at different stages by Annexin-V FITC/PI assay

B16 cells were seeded in 6-well cell culture plates (5.0×10^5 cells/well). After 12 h incubation, the medium was replaced by fresh growth media containing CPT, D-NP, or CPT-NP2. The concentration of CPT in each group was 301 nM, and the effective concentration of DM1 in D-NP and CPT-NP2 was 120 nM. The cells were incubated for 24 h and harvested with EDTA-free trypsin (0.25%). Then the cells were carefully washed by PBS and stained by Annexin-V FITC and propidium iodide (PI) according to the manufacturer's protocol. Flow cytometry was performed and data were analyzed. The cells without any treatment were utilized as a control.

QUANTIFICATION AND STATISTICAL ANALYSIS

Data analyses were performed using GraphPad Prism version 9.5 software. Data from the experiments were performed for three times or over three times. The results are expressed as the mean value ± standard deviation (mean ± SD). Statistical details of experiments can be found in the figure legends. No method was used to determine whether the data met assumptions of the statistical approach.